

1 **Revision 1**

2  
3 **Characterization of carbon phases in Yamato 74123 ureilite to constrain**  
4 **the meteorite shock history**

5 word count: 6142

6  
7 **ANNA BARBARO<sup>1</sup>, FABRIZIO NESTOLA<sup>2,3</sup>, LIDIA PITTARELLO<sup>4</sup>,**  
8 **LUDOVIC FERRIÈRE<sup>4</sup>, MARA MURRI<sup>5</sup>, KONSTANTIN D. LITASOV<sup>6</sup>, OLIVER CHRIST<sup>2</sup>,**  
9 **MATTEO ALVARO<sup>1</sup>, AND M. CHIARA DOMENEGHETTI<sup>1</sup>**

10 <sup>1</sup>Department of Earth and Environmental Sciences, University of Pavia, Via A. Ferrata 1, I-27100, Pavia, Italy

11 <sup>2</sup>Department of Geosciences, University of Padova, Via Gradenigo 6, 35131, Padova, Italy

12 <sup>3</sup>Geoscience Institute, Goethe-University Frankfurt, Altenhöferallee 1, 60323, Frankfurt, Germany

13 <sup>4</sup>Natural History Museum, Department of Mineralogy and Petrography, Burgring 7, 1010, Vienna, Austria

14 <sup>5</sup>Department of Earth and Environmental Sciences, University of Milano-Bicocca, I-20126, Milano, Italy

15 <sup>6</sup>Vereshchagin Institute for High Pressure Physics RAS, Troitsk, Moscow, 108840, Russia

16  
17 **ABSTRACT**

18 The formation and shock history of ureilite meteorites, a relatively abundant type of  
19 primitive achondrites, has been debated since decades. For this purpose, the characterization  
20 of carbon phases can provide further information on diamond and graphite formation in  
21 ureilites, shedding light on the origin and history of this meteorite group. In this work, we  
22 present X-ray diffraction and micro-Raman spectroscopy analyses performed on diamond and  
23 graphite occurring in the ureilite Yamato 74123 (Y-74123). The results show that nano- and  
24 micro-diamonds coexist with nano-graphite aggregates. This, together with the shock-  
25 deformation features observed in olivine, such as mosaicism and planar fractures, suggest that  
26 diamond grains formed by a shock event ( $\geq 15$  GPa) on the Ureilitic Parent Body (UPB). Our  
27 results on Y-74123 are consistent with those obtained on the NWA 7983 ureilite and further  
28 support the hypothesis that the simultaneous formation of nano- and micro-diamonds with the  
29 assistance of a Fe-Ni melt catalysis may be related to the heterogeneous propagation and  
30 local scattering of the shock wave. Graphite geothermometry revealed an average recorded

31 temperature ( $T_{\max}$ ) of 1314°C ( $\pm$  120°C) in agreement with previously estimated  
32 crystallization temperatures reported for graphite in Almahata Sitta ureilite.

33 **Key words:** carbon phases, diamond, graphite, ureilite meteorites, shock, impact event.

34

35

## INTRODUCTION

36 Ureilites represent the second largest group of achondrite meteorites (Goodrich et al.  
37 1992), with about 570 individuals with distinct names but only 6 observed falls (Meteoritical  
38 Bulletin Database 2020). Their formation, origin, and history are still under discussion among  
39 the scientific community. The debate about the formation of carbon phases contained in these  
40 meteorites has been going on for 80 years (see Nestola et al. 2020, and references therein).

41 As reported by Goodrich et al. (1992), ureilites appear to be fractionated ultramafic  
42 igneous rocks, either magmatic cumulates (Berkley et al. 1980; Goodrich et al. 1987) or  
43 partial melt residues (Boynnton et al. 1976; Scott et al. 1992) and, thus, the products of  
44 planetary differentiation processes. These conclusions were based on mineralogy, textures,  
45 fabrics, lithophile element chemistry, and on some aspects of Sm-Nd isotopic systematics  
46 (Berkley et al. 1976) observed in these meteorites (Goodrich et al. 1992). Ureilites strongly  
47 differ from the other groups of stony meteorites (i.e., due to a high content of carbon phases  
48 and distinct oxygen isotopic composition) and, compared to chondrites, they are enriched in  
49 Mg, but depleted in metal, troilite, and alkalis. Ureilites typically contain large olivine grains  
50 and a few smaller low Ca-clinopyroxene (pigeonite) aggregates in a fine-grained, carbon-  
51 rich, matrix. Minor phases are kamacite (1-3 vol% with the Ni content up to 7.3 %), troilite  
52 (1-2%), chromite (1-2%), and carbon material (up to 8.5%) (Cloutis et al. 2010; Goodrich et  
53 al. 2015). Carbon is present as diamond, usually with stacking disorder and nanotwins

54 (Németh et al. 2014, 2020a, 2020b; Salzmann et al. 2015; Murri et al. 2019), graphite, and  
55 organic material (e.g., Sabbah et al. 2010).

56 The different shock levels observed in ureilites are very important for constraining  
57 their history. Shock level determination in meteorites was first proposed by Stöffler et al.  
58 (1991, 2018) and is subdivided in six stages of shock for ordinary chondrites, from low (S1)  
59 to high (S6) level of shock, based on (i) shock effects in olivine and plagioclase (e.g.,  
60 extinction, fractures, planar elements) and (ii) the presence of glass and/or of high-pressure  
61 silicate phases. Recently, Nakamuta et al. (2016) adapted the shock classification based on  
62 olivine in chondrites to the observations in ureilites. For this reason, we will apply this  
63 classification in this work.

64 The occurrence of diamonds in ureilites poses the question of how this high-pressure  
65 mineral formed and whether diamonds in ureilites are similar or not to those formed by shock  
66 in terrestrial impact structures (e.g., Masaitis 1998; Hough et al. 1995; Koeberl et al. 1997;  
67 Ohfuji et al. 2015; Murri et al. 2019). Three main hypotheses have been proposed for the  
68 formation of diamonds in ureilites: (i) static high-pressure conditions in the deep interior of  
69 large parent bodies (Urey 1956), (ii) direct transformation from graphite due to shock (e.g.,  
70 Lipschutz et al. 1964; Bischoff et al. 1999; Grund and Bischoff 1999; Nakamuta et al. 2000,  
71 2016; Hezel et al. 2008; Le Guillou et al. 2010; Ross et al. 2011; Lorentz 2019), also strongly  
72 supported by De Carli et al. (1995; 2002), and (iii) growth from a dilute gas phase, i.e., at low  
73 pressure in the solar nebula by a chemical vapor deposition (CVD) process (Fukunaga et al.  
74 1987). The hypothesis of formation under static high-pressure conditions was recently  
75 supported by Miyahara et al. (2015) and Nabiei et al. (2018), who concluded that the size of a  
76 hypothetical Ureilitic Parent Body (UPB) could be comparable to the size of Mars, since  
77 static high-pressure conditions would be required for the formation of micrometer-scaled-  
78 diamond crystallites. The shock hypothesis was instead supported by the results obtained by

79 Nakamuta et al. (2016). Indeed, these authors proposed that diamonds in ureilites could have  
80 formed at high-pressure (above 12 GPa) by spontaneous shock transformation from graphite,  
81 and at low pressure (6-10 GPa) by a solid-state catalytic transformation from graphite in  
82 presence of a Fe-Ni melt. Additional support to the shock hypothesis is provided in a recent  
83 work by Nestola et al. (2020) on Almahata Sitta samples (AhS 72 and AhS 209b), as well as  
84 on NWA 7983. In their study, graphite associated with nano- and (in NWA 7983) micro-  
85 diamonds was reported, suggesting that the conversion from graphite to diamond was  
86 triggered by an impact event and was favored by the catalytic effect of Fe-Ni melts.

87 Yamato 74123 (Y-74123) ureilite is a meteorite that was found in Antarctic in 1974  
88 by the Japanese expedition on the Yamato mountains. The first detailed study of Y-74123  
89 dates back to 1978, when Hintenberger et al. (1978) measured its noble gases contents as well  
90 as several major and minor elements bulk rock abundances. Takeda et al. (1980) have  
91 reported the petrological description and a chemical characterization of pyroxenes, which  
92 revealed Fe-bearing augite compositions ( $\text{En}_{75}\text{Fs}_{18}\text{Wo}_7$ ). In addition, the magnetic properties  
93 of Y-74123 were studied by Nagata (1980). Moreover, Grady et al. (1985) carried out a C-  
94 isotopic study on Y-74123 reporting values of about  $\delta^{13}\text{C}_{\text{PDB}}=-1.7$ , well inside the range of  
95 ureilites. However, the carbon phases of Y-74123 have not been extensively studied yet.

96 In this work, we present the results of a multi-methodological study carried out on  
97 diamond and graphite aggregates observed in Yamato 74123, to understand the carbon phases  
98 formation in ureilites. In addition, a comparison with similar carbon phases in other  
99 meteorites, based on a literature survey, and a discussion on their possible formation  
100 hypothesis are also presented.

101

102

## METHODS

103           The fragment of Y-74123 (NHMV-#7636\_A) and a corresponding polished thin  
104 section (NHMV-L9822) investigated in this study were kindly provided by the Natural  
105 History Museum Vienna (Austria). The thin section was investigated by optical and electron  
106 microscopy at the Department of Earth and Environmental Science, University of Pavia  
107 (Italy). Scanning electron microscopy (SEM) of the uncoated fragment of Y-74123 was  
108 performed using a FEI Quanta 200 SEM equipped with an Energy Dispersive X-ray  
109 Spectrometry (EDS) in low vacuum mode at the CEASC (Centro di Analisi e Servizi per la  
110 Certificazione) of the University of Padova (Italy). Backscattered electron (BSE) images of  
111 Y-74123 were obtained in low vacuum mode analytical conditions, at the working distance of  
112 10.6 mm, with an emission current of 93 mA, and a voltage of 20 kV, with the aim to identify  
113 the graphite beds in which diamonds were probably located. The BSE images collected by  
114 SEM were merged and analyzed with ImageJ and MultiSpec software to estimate the relative  
115 percentages of each phase of interest observed on the surface of the investigated meteorite  
116 fragment.

117           Carbon phases were manually extracted from the fragment and mounted on the tip of  
118 a 100  $\mu\text{m}$  thick glass fiber (Fig. 1) and investigated using micro-Raman spectroscopy (MRS)  
119 followed by X-ray diffraction (XRD).

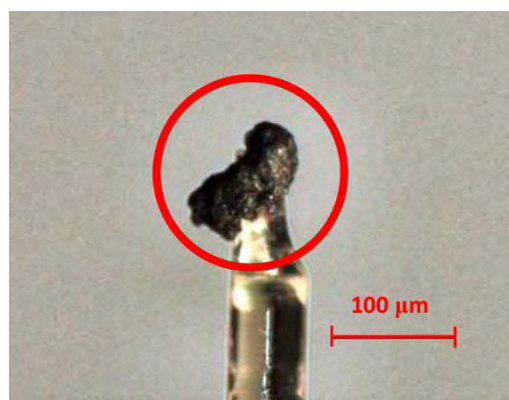


**FIGURE 1.** Carbon-bearing subsample of Y-74123 attached at the top of a glass fiber. Micro-Raman spectroscopy and XRD analyses were performed on this subsample.

120

121           Micro-Raman spectroscopy analyses were performed on the graphite material  
122 occurring in the extracted carbon-bearing subsample of Fig. 1 to estimate the recorded  
123 temperature using the geothermometer of Cody et al. (2008), modified by Ross et al. (2011).  
124 The analysis of Y-74123 graphite was performed by high-resolution MRS using a Horiba  
125 LabRam HR Evolution spectrometer equipped with an Olympus BX41 confocal microscope  
126 at the controlled temperature of 20 ( $\pm 1$ ) °C at the Department of Earth and Environmental  
127 Science of the University of Pavia. A 532 nm laser excitation with an operating power of 1-2  
128 mW (in order to prevent damage of the graphite), a grating of 600 g/mm, and a magnification  
129 of 50x was used. The spectrometer was calibrated using the silicon Raman peak at 520.5  $\text{cm}^{-1}$   
130 <sup>1</sup>. The spectral resolution was 2  $\text{cm}^{-1}$  and the acquisition time for each spectrum was 30  
131 seconds with four accumulations. Curve fitting of the spectra was carried out using the  
132 OMNIC<sup>TM</sup> software for dispersive Raman (Thermo Fisher Scientific) adopting Gaussian +  
133 Lorentzian curves to obtain the best fit. XRD analyses were then performed on the same  
134 carbon-bearing subsample (Fig. 1) using a Rigaku-Oxford Diffraction Supernova kappa-  
135 geometry goniometer with an X-ray Mo micro-source equipped with a Pilatus 200K Dectris  
136 detector in transmission mode, controlled by the Crysalis-Pro<sup>TM</sup> software at the Department  
137 of Earth and Environmental Science in University of Pavia. Line profile analysis fitting of the  
138 obtained diffraction pattern was performed using the High Score Plus Software package  
139 (Panalytical) to estimate the crystallite size.

140

141

## RESULTS

142

### **Petrographic description and observation by Scanning Electron Microscopy**

143

144

145

The investigated polished thin section of Y-74123 consists of aggregates of subhedral to  
anhedral olivine mineral grains, with varying amounts of interstitial pyroxenes and Si-Al-rich  
glass. The sample contains coarse-grained olivine and minor pigeonite crystals, ranging from

146 0.1 to 1.5 mm in size, surrounded by a large amount of opaque material (Fig. 2), composed of  
147 carbon mixed with different sulfides and metal phases. Pores and small grains of metal and  
148 sulfide ( $\leq 100 \mu\text{m}$  in size) commonly occur in the interstitial space between pyroxene and  
149 olivine grains.

150         The shock level of Y-74123 was determined using optical microscope observations on  
151 shock microstructures in olivine crystals in transmitted light and following the criteria of  
152 Stöffler et al. (1991, 2018) and Nakamuta et al. (2016). Olivine crystals show undulate  
153 extinction, planar fractures, and locally, mosaicism. The concurrent observation of undulate  
154 extinction and mosaicism in olivine indicates a pressure in the range of 15-20 GPa,  
155 corresponding to shock level S4 (Stöffler et al. 2018). In addition, both silicates, i.e., olivine  
156 and clinopyroxene, show darkening, caused by the dispersion of Fe-Ni metal and sulfides  
157 within the grains, which is commonly associated to shock metamorphism (e.g., Rubin 2006).  
158 In the investigated sample, even after a careful inspection by optical and electron microscopy,  
159 high-pressure polymorphs of olivine, such as wadsleyite or ringwoodite, were not found.

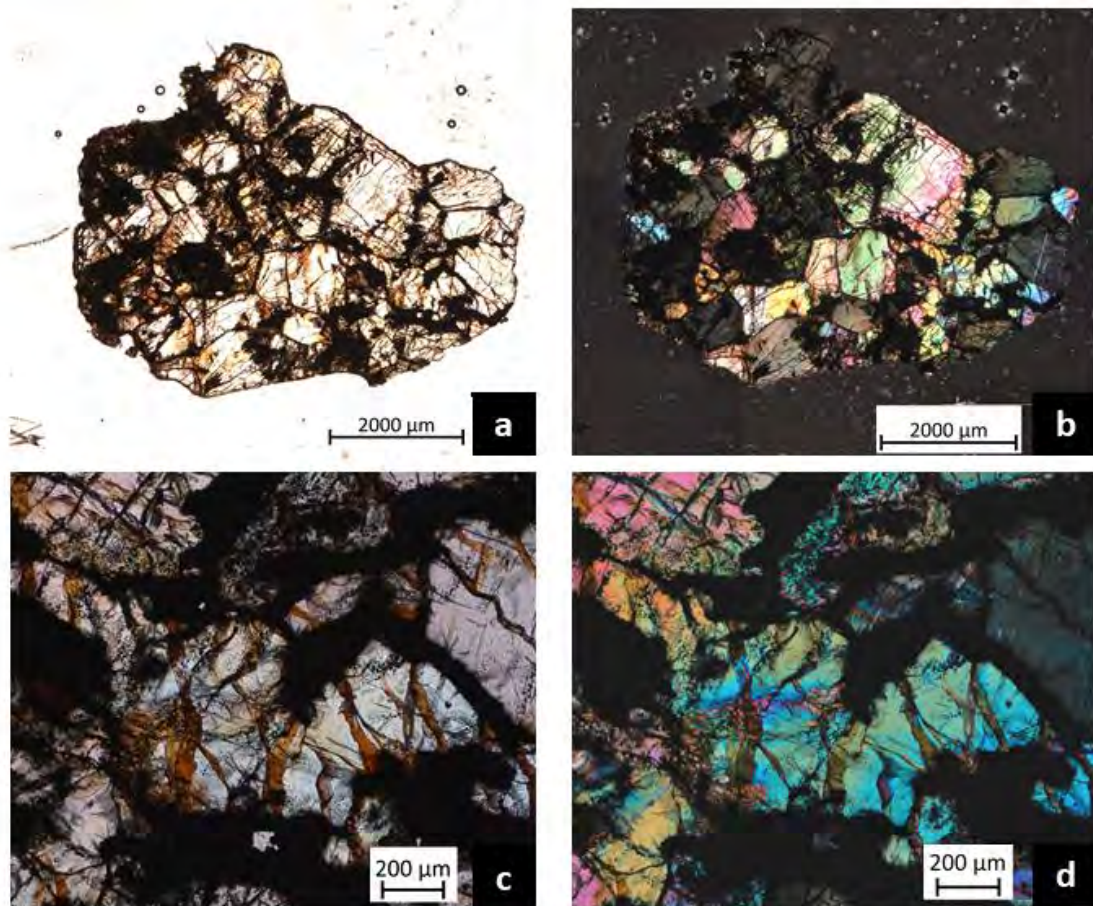


**FIGURE 2.** Yamato 74123 polished thin section (NHMV-L9822) overview in plane-polarized light (a) and between crossed polarizers (b); detailed structure of olivine grains in Y-74123 in plane-polarized light (c) and between crossed polarizers (d) are also presented. Note the presence of interstitial opaque material and the size of olivine grains, which dominate the thin section.

160 A fragment of Y-74123, about 8 x 5 x 5 mm in size, was analyzed by SEM. Figure 3a  
161 shows a BSE image of a typical carbon aggregate which occurs as interstitial phase in  
162 silicates. The size of the carbon phases in Y-74123 is evident in Fig. 3b, where carbon phases  
163 are about 10  $\mu\text{m}$  wide.

164 In Fig. 3a, it is possible to see that locally, metal phases, indicated as “Fe-Ni metal”,  
165 occur next to silicates. These metal phases are extremely fine-grained, partly mixed with the  
166 carbon phases.



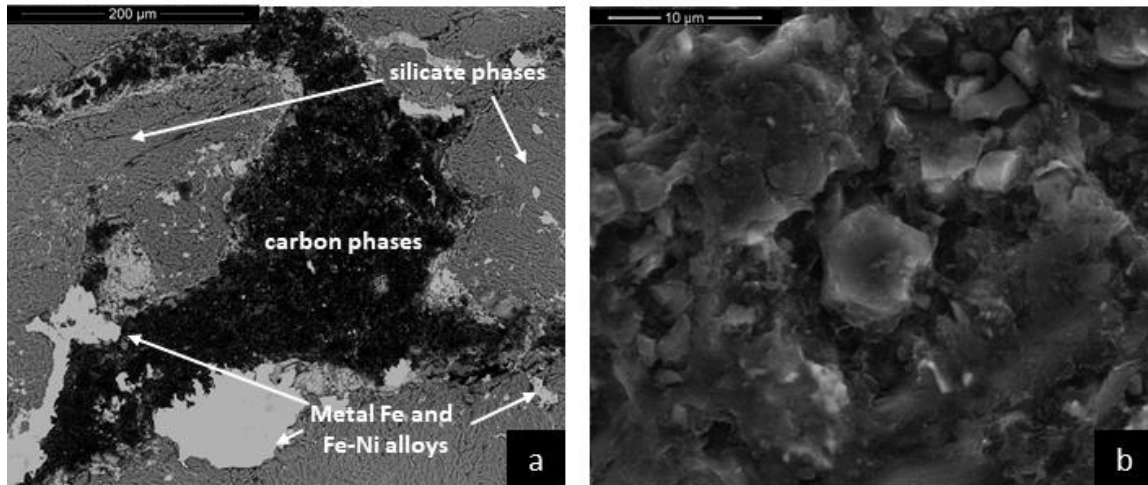


**FIGURE 3.** (a) BSE image of a carbon aggregate from which the investigated carbon-bearing subsample was extracted. Also note the presence of silicate phases and Fe-Ni metal and alloys (metal + troilite + oxide); (b) detail of (a) in secondary electron (SE). As visible on this image, the aggregates in the carbon phases beds are not larger than 10 µm in size.

167           The relative abundances, expressed in percentages, of the main mineralogical  
168 components present on the surface of the investigated sample of Y-74123 are: 91% of silicate  
169 phases (olivine and pyroxene), 7% of carbon phases, and 2% of Fe-Ni metal and alloys,  
170 respectively (Fig. 4). The image analysis performed on the surface of the fragment of Y-  
171 74123 was important to evidence the best carbon aggregate zone from which to extract the  
172 carbon-bearing aggregate to be analyzed by MRS and XRD. The investigated fragment of Y-  
173 74123 turned out to be relatively easy to be cut and polished in comparison with many other  
174 studied ureilites, indicating a relatively low amount of diamonds.

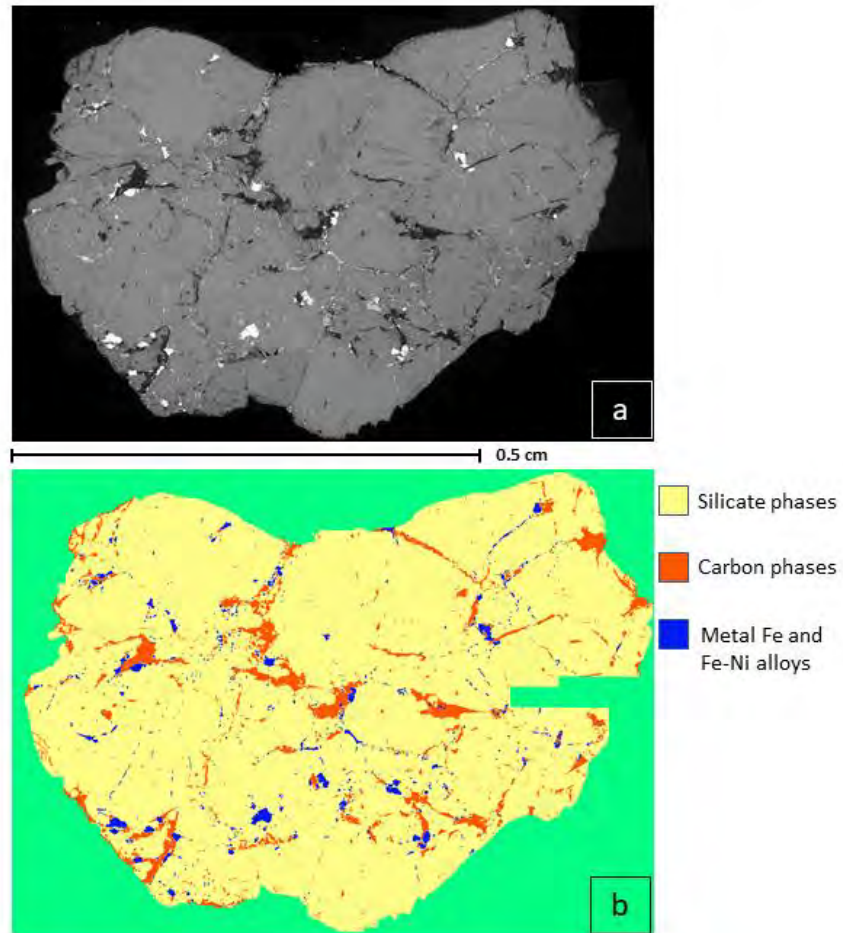


**FIGURE. 4.** (a) BSE mosaic of the Yamato 74123 fragment (NHMV-#7636\_A) showing the typical texture of the meteorite; (b) image analysis applied to (a) with the percentage referred to silicate phases, carbon phases, Fe-Ni metal, Fe-Ni alloys and Fe-oxides.

## 176 X-Ray Diffraction

177 The reconstructed XRD image of the carbon-bearing aggregate of Yamato 74123 and its  
178 powder diffraction pattern are shown in Figs. 5a and b. Instead, Fig. 5c clearly shows the  
179 presence of spots referred to micrometer sized diamond.

180 In particular, Fig. 5a shows both rings and spots at  $d$ -spacing characteristic of cubic  
181 diamond ( $d$ -spacing at 2.06 Å, 1.26 Å, and 1.07 Å) and hexagonal graphite (highest peak at  
182  $d$ -spacing at 3.34 Å, while the peaks at  $d$ -spacing 2.03 Å and 1.15 Å are overlapped by the  
183 diamond peaks). In Fig. 5b the highest peak of diamond (at  $d$ -spacing 2.06Å) shows an  
184 asymmetry. This asymmetry could be ascribed, at higher  $d$ -spacing ( $d \approx 2.18$ Å), to the  
185 presence of cubic and hexagonal  $sp^3$  stacked layers or nanotwins (Murri et al. 2019) and, at  
186 lower  $d$ -spacing ( $d \approx 2.02$  Å), to the main peak of Fe metal (which also shows peaks at  $d$ -  
187 spacing 1.42 Å and 1.17 Å). In addition to diamond, graphite, and Fe metal, a few other  
188 peaks can be assigned to troilite ( $d$ -spacing at 2.99 Å, 2.66 Å, 1.72 Å, and 1.68 Å), and also  
189 to minor silicate matrix components. The presence of cubic Ni, common in ureilites, cannot  
190 be excluded, as its peaks overlap those of metallic Fe and troilite.

191 To estimate the crystallite size of the carbon phases, we applied line profile analysis  
192 fitting to the diffraction pattern reported in Fig. 5b. The integral breadth values, which were  
193 obtained by this method, were then inserted into the Scherrer equation (Eq. 1 and 2, Scherrer  
194 1918) to estimate the crystallite size, as follows:

$$195 \quad (1) \quad \beta(2\theta) = \frac{K_{\beta} \times \lambda}{\langle D \rangle_V \cos \theta_{hkl}}$$

$$196 \quad (2) \quad \frac{D_V}{K_{\beta}} = \frac{\lambda}{\cos \theta_{hkl} \times \beta(2\theta)}$$

197 Scherrer equation provides a correlation between peaks broadening  $\beta$ , the dimension of  
198 diffracted domain, and the crystallite size ( $D_V$ ).  $K$  is a constant value ranging between 0.5 and

199 1, describing the contribution of crystallites shape and dependent upon the relative orientation  
200 of the scattering vector with respect to the external shape of the crystallite (Scherrer 1918).

201 For diamond, in order to obtain a reliable estimate of the crystallite size, we only used  
202 the two peaks at  $d$ -spacing 1.26 Å and 1.07 Å, as they do not exhibit any overlap with peaks  
203 of other phases within the analyzed carbon fragment . A similar approach was used to  
204 estimate the crystallite size of graphite, using the peak at  $d$ -spacing 3.34 Å (see Table 1). The  
205 results are reported in Table 1 along with the unit cell parameters and the space group for the  
206 diamond single crystal found in Y-74123. The possibility to estimate the unit-cell parameters  
207 for the investigated diamond in Y-74123 implies that micrometer-sized diamonds (i.e., spots  
208 in the diffraction image) are present. As it appears from the XRD images (Figs. 5a and c),  
209 i.e., on the basis of the presence of spots and rings, we can state that nano-graphite coexists  
210 with micro- and nano-diamonds in Y-74123, as also observed by Goodrich et al. (2020) and  
211 Nestola et al. (2020) in the NWA 7983 ureilite.

212

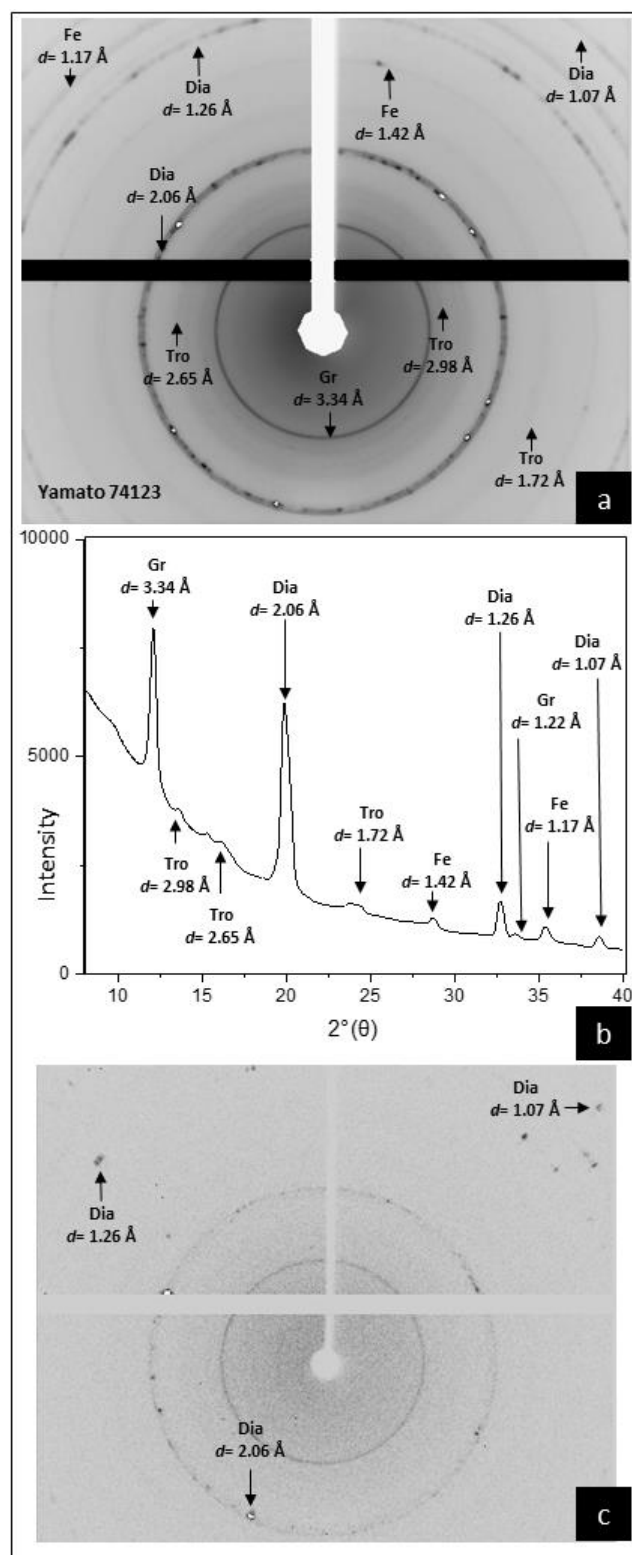


**FIGURE. 5** X-ray diffraction images of the carbon-bearing subsample from Y-74123. In (a) reconstructed powder diffraction image and in (b) X-ray diffraction pattern of the investigated sample, analyzed by micro X-ray powder diffraction, are shown. The most abundant phases found in the carbon-bearing aggregate are diamond (Dia), graphite (Gr), Fe metal (Fe), and troilite (Tro). In (c) a diffraction image shows the spots corresponding to micrometer-sized diamonds.

**Table 1.** The unit cell parameters for the micrometer-sized cubic diamond single crystal found in Y-74123. Mo  $\lambda \approx 0.71$ .  $2\theta^\circ$  positions of the graphite and diamond diffraction peaks,  $d$  spacings, and the crystallite size ( $D_v$ ) are reported. The crystallite size was calculated using the most intense peak of graphite at 3.34 Å, and the two peaks of diamond at 1.26 Å and 1.07 Å.

<b>single crystal micrometer-sized cubic diamond (sp. gr. <i>Fd-3m</i>)</b>		
$a = 3.569(1) \text{ \AA}$		
$V = 45.46(2) \text{ \AA}^3$		
<b>polycrystalline diamond</b>		
Pos. [ $2\theta^\circ$ ]	$d$ -spacing (Å)	$D_v$ (nm)
32.65	1.26	15
38.50	1.07	11
<b>polycrystalline graphite</b>		
Pos. [ $2\theta^\circ$ ]	$d$ -spacing (Å)	$D_v$ (nm)
12.10	3.34	8

## 214 Micro-Raman spectroscopy

215 We applied the geothermometric approach by Cody et al. (2008) and Ross et al. (2011),  
 216 following the same procedure as reported in Barbaro et al. (2020a, 2020b) for Almahata Sitta  
 217 samples (AhS 209b, AhS 72, and AhS A135A), to determine the  $T_{\max}$  recorded by graphite.  
 218 The temperature was estimated using Eq. 3, expressed in terms of Raman G-band full width  
 219 at half maximum (FWHM) ( $\Gamma_G$ ):

$$220 \quad (3) \quad T_{\max}(\text{°C}) = 1594.4 - 20.4\Gamma_G - 5.8 \times 10^{-2}\Gamma_G^2$$

221 In Table 2, we list the graphite peaks positions (G-band, D-band, and D' band), the relevant  
 222  $\Gamma_G$  values (G, D, and D' bands FWHM) for Y-74123, as well as the  $T_{\max}$  estimated using Eq.  
 223 3.

224 In order to compare our  $\Gamma_G$  data with those published by Ross et al. (2011) and Barbaro  
 225 et al. (2020b), we corrected our data for the instrumental peak broadening using a high-

226 quality gemstone lithospheric diamond (with  $\Gamma_G = 5 \text{ cm}^{-1}$ ), following the same procedure as  
 227 in Ross et al. (2011) (see Table 2). In Table 2, for each set of acquisition, the values of  $\Gamma_G$   
 228 used in Eq. 3 to obtain the  $T_{\max}$ , are reported.  $T_{\max}$  values range between 1265 and 1334 ( $\pm$   
 229 120) °C. These temperatures are slightly higher than those obtained by Ross et al. (2011) on  
 230 graphite in AhS #7 ureilitic fragment ( $T_{\max}$  of  $990 \pm 120$  °C), whereas they are very similar  
 231 to those obtained by Barbaro et al. (2020b) on other Almahata Sitta samples (average  $T_{\max}$  of  
 232 1266 °C for graphite in AhS 209b, 1242 °C in AhS 72, and 1332 °C in AhS A135A). A  
 233 comparison between the average temperatures recorded by graphite on the above quoted  
 234 ureilitic samples is presented in Table 3.

**Table 2.** Center positions for G, D, and D' bands and FWHM (both in  $\text{cm}^{-1}$ ) of Y-74123. Calculated crystallization temperature,  $T_{\max}$ , is reported in the last column and was obtained using the Equation 3. The uncertainty on  $T_{\max}$  is  $(2\sigma) \pm 120$  °C.

G-band center	G-band FWHM	G-band FWHM corrected	D-band center	D-band FWHM	D'-band center	D'-band FWHM	$T_{\max}$ (°C)
<b>Y-74123</b>							
1582	24	15	1356	49	1618	21	1286
1580	22	13	1354	46	1618	19	1310
1579	21	13	1349	37	1611	22	1329
1579	18	11	1356	22	1618	17	1365
1579	20	12	1351	40	1616	23	1334
1581	25	16	1350	50	1617	22	1265

235

**Table 3.** Comparison among the  $T_{\max}$  recorded by graphite in different ureilites using the geothermometer by Cody et al. (2008)\*.

	AhS #7 (Ross et al. 2011)	AhS 209 (Barbaro et al. 2020b)	AhS 72 (Barbaro et al. 2020b)	AhS A135A (Barbaro et al. 2020b)	Y-74123 (this work)
<b>Average <math>T_{\max}</math> (°C)</b>	990 $\pm$ 120	1266 $\pm$ 120	1242 $\pm$ 120	1332 $\pm$ 120	1314 $\pm$ 120

\* See Cody et al. (2008) and Ross et al. (2011) for a detailed description of the applied geothermometry. The temperature values recorded by graphite in AhS #7 sample are after Ross et al. (2011) and those recorded for AhS 209, AhS 72, and AhS A135A are from Barbaro et al. (2020b).

236

237

238 **DISCUSSION**

239           Micro-Raman spectroscopy and XRD analyses in Y-74123 revealed the presence of  
240 diamond and graphite aggregates in the interstitial space between silicate grains, as  
241 commonly observed in other ureilites (e.g., Hanneman et al. 1967; Vdovykin 1971). Our  
242 results from the XRD analysis on Y-74123 confirm the coexistence of nano- and micro-  
243 diamonds associated with nano-graphite. In the carbon-bearing aggregates, we also detected  
244 Fe metal and troilite, which fill the interstitial space between graphite-diamond crystals or  
245 occur at the border of the carbon aggregates (Fig. 4).

246           The observed local differences in size of the newly formed diamonds, i.e., nano- to  
247 micro-metric, may result from heterogeneous shock distribution within a heterogeneous  
248 sample. The heterogeneous distribution of shock effects is mainly ascribed to shock  
249 impedance contrast between contiguous phases. For greater contrast, the shock impedance is  
250 amplified (Ogilvie et al. 2011), as in the case of large, “rigid”, olivine crystals, separated by  
251 interstitial, relatively “soft”, carbon-bearing matrix. This implies that the shock pressure  
252 locally experienced by the carbon phases might have been higher than that recorded by the  
253 adjacent olivine crystal, thus, explaining the local occurrence of relatively coarse-grained  
254 diamonds. Conversely, for cases of low contrast between phases, the shock impedance would  
255 have been suppressed. Furthermore, we cannot exclude that Y-74123 suffered multiple  
256 impact events with different P-T conditions.

257           Our study provides further evidence in support of the diamond formation mechanism  
258 in ureilites proposed for NWA 7983 ureilite by Nestola et al. (2020). According to this  
259 mechanism, the formation of micrometer-sized diamond crystals from graphite observed in  
260 Y-74123 is likely due to the combined effect of highly heterogeneous P-T-conditions due to  
261 shock wave propagation and immediate penetration of Fe-Ni melt into carbon aggregates,



262 whereas the formation of nano-diamonds resulted from direct transformation from graphite  
263 (i.e., even without the catalytic Fe-Ni melt). The occurrence of Fe compounds, as observed in  
264 Y-74123, could explain the formation of diamonds at pressures  $\geq 15$ -20 GPa (Nestola et al.  
265 2020), which is lower than the pressure of 30-60 GPa estimated for diamonds formed in  
266 impact cratering processes on Earth (see, e.g., Koeberl et al. 1997, and references therein). In  
267 Nestola et al. (2020) it is clearly reported how the catalyzed formation of diamonds by  
268 metallic melts during a shock event can also account for simultaneous formation of micro-  
269 and nanodiamonds in ureilites. These authors, with the aim to explain this process, reported  
270 an example of a pulsed heating experiment performed on a graphite-metal charge in a static  
271 high-pressure apparatus (Varfolomeeva 1971). This apparatus simulates natural impact  
272 processes (De Carli et al. 2002; Bundy et al. 1967) which produced diamonds up to 10- $\mu$ m-  
273 sized, found near to the catalyst, and nanodiamonds occurring in other parts of the  
274 experimental charge (Nestola et al. 2020 and references therein).

275         The proposed scenario is further supported by the average value of the temperatures  
276 determined for Y-74123 graphite [ $T_{\max}=1314^{\circ}\text{C}$  ( $\pm 120^{\circ}\text{C}$ )], which is similar to the values  
277 reported by Barbaro et al. (2020a; 2020b) for Almahata Sitta samples (e.g., AhS 209b, AhS  
278 72, and AhS A135A), even though slightly higher than the values reported by Ross et al.  
279 (2011) for the AhS #7 sample. As reported by Gillet and El Goresy (2013), the shock peak  
280 temperature determination for a sample with different mineral composition should also  
281 account for the effect of the porosity, grain boundaries, and heterogeneous composition of the  
282 rock. In addition, it is important to consider that the shock waves do not propagate at the  
283 same speed in all different minerals of a polymineralic rock, as explained above. However,  
284 even if it is difficult to estimate the exact peak shock pressure values of the impact event(s),  
285 we can argue that the temperature recorded by graphite may correspond to the shock-induced  
286 temperature or to a subsequent post-shock thermal event, as hypothesized by Gillet and El

287 Goresy (2013). We exclude that our estimated temperature values could be a pre-shock  
288 temperature, because our estimation is determined on newly crystallized nano-graphite. Such  
289 nano-graphite cannot be the pristine graphite of the UPB, which should have been  
290 micrometer-sized, due to the long residence time spent in the UPB deep interior. Therefore,  
291 as reported by Barbaro et al. (2020b) for three AhS ureilitic fragments, nano-graphite formed  
292 by shock.

### 293 **Implications**

294 Our study on carbon phases in Yamato 74123 provides hints on the shock history of  
295 this specific meteorite, and generally, of the UPB. The XRD analysis carried out on Y-74123  
296 showed that nano-diamonds coexist together with micro-diamonds and nano-graphite, in  
297 agreement with observations by Nestola et al. (2020) on the NWA 7983 ureilite meteorite. In  
298 addition, by means of MRS analyses of graphite, we were able to show that (i) the  
299 investigated sample exhibits homogeneous values of G-band centers (between 1579 and 1582  
300  $\text{cm}^{-1}$ ) and D-band centers (between 1349 and 1356  $\text{cm}^{-1}$ ) and that (ii) the  $\Gamma_G$  of graphite for  
301 the G-band range between 11 and 16  $\text{cm}^{-1}$ . These values were used to estimate an average  
302  $T_{\text{max}}$  of 1314°C ( $\pm 120$  °C).

303 Our results support that micrometer-sized diamonds in Y-74123, as also suggested by  
304 Nestola et al. (2020) for NWA 7983, formed with the assistance of the catalytic effect of  
305 metallic melts, without requiring static high-pressures conditions within a large Mars-sized  
306 parent body. The formation of micro- and nano-diamonds and nano-graphite is likely to be  
307 the result of an impact event or multiple impact events. We assume that the temperature  
308 recorded by graphite, close to 1200-1300°C, likely represents the shock-induced temperature  
309 excursion or corresponds to a subsequent post-shock temperature. The temperature values  
310 obtained in our sample Y-74123, together with further studies on ureilites, using the same

311 approach as presented here, will contribute to widen our knowledge of the graphite resetting  
312 temperatures by shock.

313 In conclusion, the results from our combined SEM, XRD, and MRS study in Y-74123  
314 suggest that one or multiple shock event(s), with the contribution of metallic melts catalysis,  
315 is likely responsible for the formation of diamond, both nano- and micro-diamonds.  
316 Moreover, heterogeneity in the peak shock pressure that affected the UPB during the impact  
317 event(s) may also explain the coexistence of diamonds with notable different sizes.

318

319

320

### **Acknowledgements**

321 This paper is dedicated to the memory of Heinrich Hintenberger (1910–1990) who donated to  
322 the NHM Vienna collection the Yamato 74123 sample used for this study. C.A. Goodrich is  
323 acknowledged for interesting discussions. S. Jaret and an anonymous reviewer are thanked  
324 for their comments, which greatly contributed improving this manuscript. S. Redfern is  
325 thanked for editorial handling. This work was supported by PNRA 2018 grant number  
326 PNRA18 00247 – A to F. N.; A.B., M.C.D., M.M., and M.A. were funded by the IMPACT  
327 project (R164WEJAHH) to M. Alvaro.

328

329 **References**

- 330 Barbaro, A., Domeneghetti, M. C., Goodrich, C. A., Meneghetti, M., Litti, L., Fioretti, A. M.,  
331 Shaddad, M. H., Alvaro, M., and Nestola, F. (2020a) Shock temperature recorded by graphite  
332 in ureilites from Almahata Sitta. 51<sup>st</sup> Lunar and Planetary Science Conference, abstract #1480.
- 333 Barbaro, A., Domeneghetti, M. C., Goodrich, C., Meneghetti, M., Litti, L., Fioretti, A. M., Jenniskens,  
334 P., Shaddad, M. H., Alvaro, M., and others. (2020b) Graphite based geothermometry on  
335 Almahata Sitta ureilites meteorites. Minerals, submitted.
- 336 Berkley, J.L., Brown, IV, H.G., Keil, K., Carter, N.L., Mercier, J.-C.C., and Huss, G. (1976) The  
337 Kenna ureilite: an ultramafic rock with evidence for igneous, metamorphic, and shock origin.  
338 *Geochimica et Cosmochimica Acta*, 40, 1429–1437.
- 339 Berkley, J. L., Taylor, G. J., Keil, K., Harlow, G. E., and Prinz, M. (1980) The nature and origin of  
340 ureilites. *Geochimica et Cosmochimica Acta*, 44, 1579–1597.
- 341 Bischoff, A., Goodrich, C.A., and Grund T. (1999) Shock-induced origin of diamond in ureilites. 30<sup>st</sup>  
342 Lunar and Planetary Science Conference, abstract #1100.
- 343 Boynton, W. V, Starzyk, P. M., and Schmitt, R. A. (1976) Chemical evidence for the genesis of the  
344 ureilites, the achondrite Chassigny and the nakhlites. *Geochimica et Cosmochimica Acta*, 40,  
345 1439–1447.
- 346 Bundy, F. P., and Kasper J. S. (1967) Hexagonal diamond—A new form of carbon. *Journal of*  
347 *Chemical Physics*, 46, 3437–3446.
- 348 Cloutis, E. A., Hudon, P., Romanek, C. S., Bishop, J. L., Reddy, V., Gaffey, M. J., and Hardersen, P.  
349 S. (2010) Spectral reflectance properties of ureilites. *Meteoritics & Planetary Science* 45, 10–11.
- 350 Cody, G. D., Alexander, C. M. O'D., Yabuta, H., Kilcoyne, A. L. D., Araki, T., Ade, H., Dera, P.,  
351 Fogel, M., Militzer, B., and Mysen, B. O. (2008) Organic thermometry for chondritic parent  
352 bodies. *Earth and Planetary Science Letters*, 272, 446–455.
- 353 De Carli, P.S. (1995) Shock wave synthesis of diamond and other phases. *Material Research and*  
354 *Society Symposium Proceedings*, 383, 21–31.
- 355 De Carli, P. S., Bowden, E., Jones, A. P., and Price, G. D. (2002) Laboratory impact experiments  
356 versus natural impact events. In *Catastrophic Events and Mass Extinctions: Impacts and*  
357 *Beyond*, Geological Society of America Special Paper 356, p. 595–605. Lunar and Planetary  
358 Institute, Houston, Texas.
- 359 Frondel, C. and Marvin, U. B. (1967) Lonsdaleite, a hexagonal polymorph of diamond. *Nature*, 214,  
360 587–589.
- 361 Fukunaga, K., Matsuda, J., Nagao, K., Miyamoto, M., and Ito, K. (1987) Noble-gas enrichment in  
362 vapour-growth diamonds and the origin of diamond in ureilites. *Nature*, 328, 141–143.
- 363 Gillet, P. and El Goresy, A. (2013) Shock events in the Solar System: The message from minerals in  
364 terrestrial planets and asteroids. *Annual Review of Earth and Planetary Sciences*, 41, 247–285.
- 365 Goodrich, C. A., and Jones, J. H. (1987) Origin and evolution of the ureilite parent magmas: Multi-  
366 stage igneous activity on a large parent body. *Geochimica et Cosmochimica Acta*, 51, 2255–  
367 2273.

- 368 Goodrich, C. A. (1992) Ureilites: A critical review. *Meteoritics & Planetary Science*, 27, 327–352.
- 369 Goodrich, C. A., Hartmann, W. K., O'Brien, D.P., Weidenschilling, S. J., Wilson, L., Michel, P., and  
370 Jutzi, M. (2015) Origin and history of ureilitic material in the solar system: The view from  
371 asteroid 2008 TC<sub>3</sub> and the Almahata Sitta meteorite. *Meteoritic & Planetary Science*, 50, 782–  
372 809.
- 373 Goodrich, C. A., Nestola, F., Jakubek, R., Erickson, T., Fries, M., Fioretti, A. M., Ross, D. K., and  
374 Brenker, F. E. (2020) The origin of diamond in ureilites. 51<sup>st</sup> Lunar and Planetary Science  
375 Conference, abstract #1411.
- 376 Grady, M. M., Wright, I. P., Swart, P. K., and Rllinger, C. T. (1985) The carbon and nitrogen isotopic  
377 composition of ureilites: implications for their genesis. *Geochimica et Cosmochimica Acta*,  
378 49, 903–915.
- 379 Grund, T. and Bischoff, A. (1999) Cathodoluminescence properties of diamonds in ureilites: further  
380 evidences for a shock-induced origin. 62<sup>nd</sup> Annual Meteoritical Society Meeting, abstract  
381 #5074.
- 382 Hanneman, R. E., Strong, H. M., and Bundy, F. P. (1967) Hexagonal diamonds in meteorites:  
383 Implications. *Science*, 155, 995–997.
- 384 Hezel, D. C., Dubrovinsky, L., Nasdala, L., Cauzid, J., Simionovici, A., Gellissen, M., and  
385 Schonbeck, T. (2008) In situ micro-Raman and X-ray diffraction study of diamonds and  
386 petrology of the new ureilite UAE 001 from the United Arab Emirates. *Meteoritics & Planetary  
387 Sciences*, 43, 1127–1136.
- 388 Hintenberger, H., Jochum, K.P., Braun, O., Christ, P., and Martin, W. (1978) The Antarctic meteorite  
389 Yamato 74123 — a new ureilite. *Earth and Planetary Science Letters*, 40, 187–193.
- 390 Hough, R. M., Gilmour, I., Pillinger, C. T., Arden, J.W., Gilkess, K. W. R., Yuan, J., and Milledge, H.  
391 J. (1995) Diamond and silicon carbide in impact melt rock from the Ries impact crater. *Nature*  
392 378,41–44.
- 393 Koeberl, C., Masaitis, V. L., Shafranovsky, G. I., Gilmour, I., Langenhorst, F., and Schrauder, M.  
394 (1997) Diamonds from the Popigai impact structure, Russia. *Geology*, 25, 967–970.
- 395 Le Guillou, C., Rouzaud, J. N., Remusat, L., and Bourot-Denise, A. (2010) Structures, origin and  
396 evolution of various carbon phases in the ureilite Northwest Africa 4742 compared with  
397 laboratory-shocked graphite. *Geochimica et Cosmochimica Acta*, 74, 4167–4185.
- 398 Lipschutz, M. E. (1964) Origin of Diamonds in the Ureilites. *Science*, 143, 1431–1434.
- 399 Lorentz, C.A., Shiryayev, A. A., Vlasov, I. I., and Borisovsky, S. E. (2019) Metamorphism of four  
400 desert ureilites and luminescence spectroscopy of defects in ureilitic diamonds. *Meteoritics and  
401 Planetary Science*, 54, 1197–1214.
- 402 Masaitis, V. L. (1998) Popigai crater: Origin and distribution of diamond-bearing impactites.  
403 *Meteoritics and Planetary Science*, 33, 349–359.
- 404 Meteoritical Bulletin Database (2020). Available: <https://www.lpi.usra.edu/meteor/>
- 405 Miyahara, M., Ohtani, E., El, A., Lin, Y., Feng, L., Zhang, J., Gillet, P., Nagase, T., and Muto, J.  
406 (2015) Unique large diamonds in a ureilite from Almahata Sitta 2008 TC 3 asteroid. *Geochimica  
407 et Cosmochimica Acta*, 163, 14–26.

- 408 Murri, M., Smith, R. L., McColl, K., Hart, M., Alvaro, M., Jones, A. P., Németh, P., Salzmann, C. G.,  
409 Corà, F. and others. (2019) Quantifying hexagonal stacking in diamond. *Scientific Reports* 9,  
410 10334. <https://doi.org/10.1038/s41598-019-46556-3>
- 411 Nabiei, F., Badro J., Dennenwaldt T., Oveisi E., Cantoni M., Hébert C., Goresy A. El, Barrat J., and  
412 Gillet P. (2018) A large planetary body inferred from diamond inclusions in a ureilite meteorite.  
413 *Nature Communications*, 9, 1–6.
- 414 Nagata, T. (1980) Magnetic classification of Antarctic meteorites. *Proceedings of the 21<sup>st</sup> Lunar and*  
415 *Planetary Science Conference*, p. 1789–1799. Lunar and Planetary Science Institute, Houston,  
416 Texas.
- 417 Nakamuta, Y., and Aoiko, Y. (2000) Mineralogical evidence for the origin of diamond in ureilites.  
418 *Meteoritics and Planetary Science*, 35, 487–493.
- 419 Nakamuta, Y., Kitajima, F., and Shimada, K. (2016) In situ observation, X-ray diffraction and Raman  
420 analyses of carbon minerals in ureilites: Origin and formation mechanisms of diamond in  
421 ureilites. *Journal of Mineralogical and Petrological Sciences*, 111, 252–269.
- 422 Németh, P., Garve, L. A. J., Aoki, T., Dubrovinskaia, N., Dubrovinsky, L., and Buseck, P. R. (2014)  
423 Lonsdaleite is faulted and twinned cubic diamond and does not exist as a discrete material.  
424 *Nature Communications*, 5, 5447, 1–5.
- 425 Németh, P., McColl, K., Smith, R. L., Murri, M., Garvie, L. A. J., Alvaro, M., Péc, B., Jones, A. P.,  
426 Corà, F., Salzmann and others. (2020a) Diamond-graphene composite nanostructures.  
427 *Nanoletters*, 20, 3611–3619.
- 428 Németh P., McColl, K., Garvie L. A. J., Salzmann C. G., Murri M., McMillan P. F. (2020b) Complex  
429 nanostructures in diamond. *Nature Materials*, 1–6. <https://doi.org/10.1038/s41563-020-0759-8>
- 430 Nestola, F., Goodrich, C. A., Morana, M., Barbaro, A., Jakubek, R. S., Chris, O., Brenker, F. E.,  
431 Domeneghetti, M. C., Dalconi, M. C. and others. (2020) Impact shock origin of diamond in  
432 ureilite meteorites. *Proceedings of the National Academy of Sciences of the United States of*  
433 *America*, 1-9. <https://doi.org/10.1073/pnas.1919067117>
- 434 Ogilvie, P., Gibson, R. L., Reimold, W. U., Deutsch, A., and Hornemann, U. (2011) Experimental  
435 investigation of shock metamorphic effects in a metapelitic granulite: The importance of shock  
436 impedance contrast between components. *Meteoritics & Planetary Science*, 46, 1565–1586.
- 437 Ohfuji, H., Itifune, T., Litasov, K. D., Yamashite, T., Isobe, F., Afanasiev V. P., and Pokhilenko N. P.  
438 (2015) Natural occurrence of pure nano-polycrystalline diamond from impact crater. *Scientific*  
439 *Reports*, 5, 14702, 1–8.
- 440 Ross, A. J., Steele, A., Fries, M. D., Kater, L., Downes, H., Jones, A. P., Smith, C. L., Jenniskens, P.  
441 M., Zolensky, M. E., and Shaddad, M. H. (2011) MicroRaman spectroscopy of diamond and  
442 graphite in Almahata Sitta and comparison with other ureilites. *Meteoritics & Planetary*  
443 *Science*, 46, 364–378.
- 444 Rubin, A. (2006) Shock, post-shock annealing, and post-annealing shock in ureilites. *Meteoritics &*  
445 *Planetary Science*, 41, 125–133
- 446 Sabbah, H., Morrow, A. L., Jenniskens, P., Shaddad, M. H., and Zare, R. N. (2010) Polycyclic  
447 aromatic hydrocarbons in asteroid 2008 TC<sub>3</sub>: Dispersion of organic compounds inside asteroids.  
448 *Meteoritics & Planetary Science*, 45, 1710–1717.

- 449 Salzmann, C. G., Murray, B. J., and Shephard, J. J. (2015) Extent of stacking disorder in diamond.  
450 Diamond and Related Materials, 59, 69–72.
- 451 Scherrer, P. (1918) Estimation of the size and internal structure of colloidal particles by means of  
452 röntgen. Journal of Mathematical Physics, 2, 98–100.
- 453 Scott E. R. D., Keil K., and Taylor G. J. (1992) Origin of ureilites by partial melting and explosive  
454 volcanism on carbon-rich asteroids. Proceedings of the 23<sup>rd</sup> Lunar and Planetary Science  
455 Conference, pp. 1253–1254.
- 456 Stöffler, D., Keil, K., and Edward, R. D. S. (1991) Shock metamorphism of ordinary chondrites.  
457 Geochimica et Cosmochimica Acta, 55, 3845–3867.
- 458 Stöffler, D., Hamann, C., and Metzler, K. (2018) Invited Review Shock metamorphism of planetary  
459 silicate rocks and sediments: Proposal for an updated classification system. Meteoritics &  
460 Planetary Science, 49, 5–49.
- 461 Takeda, H., Mori, H., Keizo, Y., and Shiraishi, K. (1980) Mineralogical examination of the Allan  
462 Hills achondrites and their bearing on the parent bodies. Memoirs of National Institute of Polar  
463 Research. Special issue, 17, 119–144.
- 464 Urey, H. C. (1956) Diamond, meteorites, and the origin of the solar system. American Astronomical  
465 Society, 623–637.
- 466 Varfolomeeva, T. D. (1971) Synthesis and investigation of polycrystalline diamond. PhD thesis,  
467 Institute for High Pressure Physics, USSR Academy of Sciences, 154.
- 468 Vdovykin, G. (1970) Ureilites. Space Science Reviews, 10, 483–510.  
469